國立交通大學

物　　理　　研　　究　　所

碩　士　論　文

香港仔隧道實驗室宇宙射線感應中子之研究

Estimation of Neutron Yield by Cosmic Muons in Aberdeen Tunnel Laboratory

研 究 生：葉永順

指導教授：林貴林 教授

中　華　民　國　九　十　六　年　七　月

香港仔隧道實驗室宇宙射線感應中子之研究

Estimation of Neutron Yield by Cosmic Muons in Aberdeen Tunnel Laboratory

研 究 生 ： 葉永順　　Student: Yung-Shun Yeh

指導教授 ： 林貴林　　Advisor: Guey-Lin Lin

國立交通大學

物理研究所

碩士論文

A Thesis

Submitted to Institute of Physics

National Chiao Tung University

in Partial Fulfillment of the Requirements

for the Degree of

Master

in

Physics

July, 2007

Hsinchu City, Taiwan, Republic of China

中華民國九十六年七月

香港仔隧道實驗室宇宙射線感應中子之研究

學生： 葉永順　　指導教授 ： 林貴林

國立交通大學物理研究所

摘　　要

物理學家計劃在大亞灣興建一個實驗室以量測微中子最後的混合角 θ_{13}。由於微中子不容易被量測到的特性，我們必須要仔細地研究其周遭的背景以降低背景在實驗方面所造成的誤差。香港仔隧道實驗室座落在香港島上鄰近大亞灣，岩石結構與大亞灣附近的山相似，所以非常適合來研究背景。本論文主要的研究宇宙射線所造成的中子背景，我們利用模擬軟體去估計宇宙射線感應產生的中子流量並加以公式化，利用得到的公式估計香港仔隧道實驗室所得到中子流量，並比較不同模擬軟體間的差異。進一步，我們模擬香港仔隧道真實環境。在香港載隧道實驗取數前，對宇宙射線感應的中子流量，以上的結果可以給我們一個合理的預測。

Estimation of Neutron Yield by Cosmic Muons in Aberdeen Tunnel Laboratory

Student: Yung-Shun Yeh Advisor: Guey-Lin Lin

Submitted to Institute of Physics
National Chiao Tung University

ABSTRACT

Physicists prepare to measure the last unknown mixing angle θ_{13} of neutrino in Daya Bay Reactor Neutrino Experiment. Due to the difficult detection of neutrinos, it is necessary to study backgrounds carefully to reduce errors coming from the backgrounds. The Aberdeen Tunnel Laboratory, which is located near Daya Bay and have similar rock compositions as the mountains around Daya Bay, have the advantage to study backgrounds. In this thesis, we mainly focus on the cosmic moun-induced neutron background. We compare the the neutron production rate between three simulation tool kits, FLUKA 2006.3, FLUKA 1999, and Geant4, and obtain a parameterizaion formula using FLUKA 2006.3. The neutron yield in Aberdeen Tunnel Lab can be estimated via the parameterization formula. Futhermore, we ha estimate the neutron yield by cosmic muons by relastic simulation in Aberdeen Tunnel Lab. These two results give us a resonable prediction of the Aberdeen Tunnel Experiment.

致　謝

感謝指導老師林貴林老師在研究方面的指引與教導，也謝謝Group裡的王正祥老師、黃明輝老師平日對我的一些錯誤觀念有所釐清。謝謝林及仁老師在口試上點出我的一些「理所當然」，物理的觀念不應該有「理所當然」。

在研究工作進行的時候，很感謝香港團隊的Raymond Tsang、Antony Luk在研究工作上的討論與建議。 也謝謝網路上的熱心人Lindley Winslow、Alfred Tang與Marco Mauri還有同步輻射中心的許榮鈞許組長對於FLUKA的一些技術上的支援。

感謝Group裡劉宗哲學長平日對我的照顧，平日的討論使得我的一些高能物理的常識有所增加。最後感謝所上裡的伙伴、學長姊、學弟妹，平日的相處，相互鼓勵，使得我研究之路不孤單。

Contents

中文摘要 **ii**

Abstract **iii**

致謝 **iv**

1 Introduction **1**

1.1 Brief history of neutrino 2

1.2 Neutrino Oscillation 4

1.2.1 Neutrino Oscillation in Vacuum[10] 4

2 The Daya Bay Experiment **9**

2.1 The Optimization of Detector Baseline 10

2.2 Detection of $\bar{\nu}_e$ from Nuclear Reactor 12

2.3 The Aberdeen Tunnel Experiment 13

3 Estimation of the muon-induced neutrons **15**

3.1 Background to Reactor Antineutrino Experiments 16

3.1.1 Origins of the fast neutrons 17

3.2 Simulation of neutron production in hydrocarbon scintillator 18

3.3 Results 21

3.3.1 The neutron yield 21

3.3.2 Neutron energy spectra 23

3.3.3 The neutron angular distribution 26

3.3.4 Origins of neutrons 27

4 The Prediction of Neutron Yield by Cosmic Muons in Aberdeen Tunnel Site 30

4.1 Cosmic-ray Muon Distribution in Aberdeen Tunnel Site 30

4.2 Neutron yield in Aberdeen Tunnel site 33

4.2.1 Configuration 33

4.2.2 Results 34

5 Conclusion and Outlook 36

List of Figures

1.1 Energy distribution of the electrons 2

2.1 Default configuration of the Daya Bay experiment, optimized for best sensitivity in $\sin^2 2\theta_{13}$. Four detector modules are deployed at the far site and two each at each of the near sites. 10

2.2 Reactor antineutrino survival probability as a function of distance from source. The black curve is the total disappearance probability, the red curve is the term P_{12} in disappearance probability, and the blue curve is the term P_{13} in disappearance probability. 11

2.3 Schematic of antineutrino detector. An antineutrino interacts with a proton to give out a neutron and positron. Both particles produced then give out gamma rays. 13

2.4 The detector configuration for studying the cosmic background at the Aberdeen Tunnel Laboratory. 14

3.1 The Feynman diagram for a muon spallation process. 18

3.2 The histogram for neutron production positions by 10 GeV muons. It shows that the muon cascades reach equilibrium after the position 450 cm, the muon cascades reach equilibrium. 19

3.3 Illustration of neutron-induced neutron interaction 20

3.4 The neutorn yield as the function of muon energy. The horizontal axis is muon energy and the vertical axis is the events number per g-cm^{-2} per muon. The circle points are the data points of FLUKA 2006.3 and the black curve is the fitting. The red curve is the parameterization published by Wang et al.[13]. The square points are the data points of the Geant 4.8.2 and the blue dash line is the fitting. 21
3.5 Neutron energy spectra at different primary muon energy: The black histograms are results of FLUKA 2006.3. The red curves are the empirical function of Wang et al.. 24
3.6 Neutron energy spectra at different primary muon energy obtained by Wang et al.. 25
3.7 Neutron angular distribution. The horizontal axis is cosine of the angle between muon direction and neutron direction, and the vertical axis is the event number per bin. The histogram is the result of FLUKA 2006.3 and the red curves are the parameterization of Wang et al.. 26
3.8 origins of neutrons sinulated by FLUKA 2006.3 27
3.9 Origins of neutrons simulated by Geant4 28

4.1 Aberdeen Mountain 3D scheme 31
4.2 Muon energy sepctrum in Aberdeen Tunnel site 32
4.3 Muon angular distribution at the Aberdeen Tunnel site 32
4.4 The energy distribution of muon-indued neutron which contain neutrons transporting into liquid scintillator and those produced in liquid scintillator. The mean energy is 81.9 MeV. 35

List of Tables

3.1 The deviations on neutron yield predictions between two different simulation tool kits at the different experimental sites. 22

Chapter 1

Introduction

Neutrino, which has been considered one of fundamental paticles, play a very important role in both microscopic view of particle physics and the macroscopic view of the evolution of the Universe. The last decade has seen a tremendous advance in the understanding of the neutrino sector. There is now a robust evidence for neutrino flavor conversion from solar, atmospheric[1, 2], reactor[5, 6] and accelerator[3, 4] experiments, using a wide variety of detector technologies. The only consistent explanation for these results is that neutrinos are massive and that the neutrino mass eigenstates are not the same as the flavor eigenstates (neutrino mixing). Neutrino oscillations depend on two mass-squared differences and three neutrino mixing angles and one CP violation phase δ_{cp}. Four of these parameters have been measured with reasonable precision by solar, atmospheric, reactor and accelerator neutrino experiments. The last two parameters, the CP violation phase δ_{cp} and the mixing angle θ_{13}, which have not been measured precisely, become the main targets of the next generation of neutrino experiments. Even the value of θ_{13} determines whether δ_{cp} can be measured via neutrino oscillation experiments or not. Therefore, measuring θ_{13} precisely has become one of the most crucial tasks in neutrino physics.

The Daya Bay Experiment[7] propose to perform a precision measurement of θ_{13} by searching for the disappearance of electron antineutrinos from the nuclear

reactor complex in Daya Bay, China. The goal of the Daya Bay experiment is to reach a sensitivity of 0.01 or better in $\sin^2 2\theta_{13}$.

Before the mixing angle can be measured, the neutrinos have to be detected first. Neutrino detection experiments require extremely sensitive equipment and complex data acquisition system in order to discriminate signal and backgrounds from the surrounding. However, some background cannot be distinguished from neutrino events. This thesis aims to simulate the cosmic muon-induced neutron background in the laboratory at Aberdeen Tunnel, Hong Kong, which is the prototype experiment of Daya Bay project[8].

1.1 Brief history of neutrino

Neutrino was first postulated in 1930 by Wolfgang Pauli to explain conservation of energy in beta decay, the decay of a neutron into one electron and one proton. Physicists before 1930 believe the nuclei decay only emit electrons and protons. From the basic conservations of energy and momentum, the emitted electron should have a fixed energy. However, the experiment result is not consistent with physicists' expectation. The emitted electrons carry with a continuous energy spectrum, as shown in Fig. 1.1.

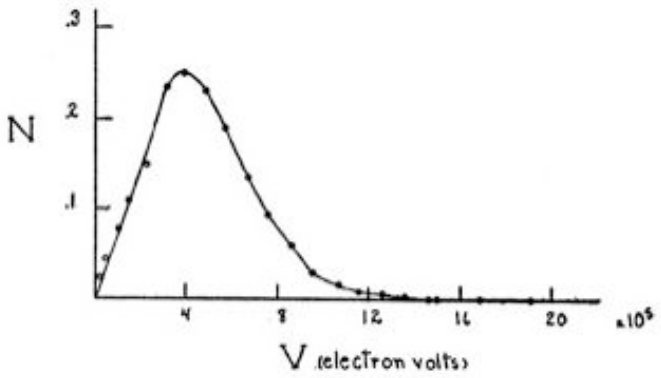

Figure 1.1: Energy distribution of the electrons

Pauli postulated that an undetected particle carries away the difference between the energy and momentum of the initial and final particles. Hence the conservation laws of energy and momentum in beta decay reaction can be maintained. Pauli assume the particle, which we call it as neutrino today, has zero mass and it is very difficult to detect. Today, due to the effort of physicists, we have known neutrino has non-zero mass and detectable. Reines and Cowan performed a historical experiment in 1956 to confirm the existence of free neutrinos, using the Savannah River nuclear reactor as a neutrino source. The following reaction is the inverse beta decay

$$\bar{\nu} + p \rightarrow n + e^{+} \tag{1.1}$$

is used to capture the antineutrino from nuclear reactor interact with a target proton to produce a neutron and a positron. Due to the cross section of neutrino and proton is only 10^{-44} cm^2, this experiment need strong neutrino source and enormous protons to be targets.

In 1962, L. Lederman, M. Schwartz, J. Steinberger and their collaborators discovered the second type of neutrino, which is named ν_μ by them, to distinguish it from the previous one, ν_e. Until 2000, the third type of neutrino, ν_τ, was eventually eventually observed directly by Fermi National Laboratory. Today, 3 types of neutrino are confirm to exist.

It is believed that neutrino has a zero mass until the Super-Kamiokande experiment[9] in 1998 which ruled out this hypothesis by observing the atmospherical neutrino oscillations. Neutrino oscillation is a quantum mechanical phenomenon whereby a neutrino created with a specific lepton flavor(electron, muon or tau) can later be measured to have a different flavor. The probability of measuring a particular flavor for a neutrino varies periodically as it propagates. The phenomenon is due to the difference between the flavor eigenstates and mass eigenstates. It also requires the non-degeneracy of mass eigenstates. This phenomenon give us a circumstantial evidence that neutrino should have non-zero masses. The neutrino oscillation phenomenon depend on 6 parameters of which two are mass-squared differences, three are mixing angle, one is CP violation phase. The Daya Bay ex-

periment propose to measure the one of the mixing angles in neutrino oscillation. More detail about neutrino oscillation will be introduced in following material.

1.2 Neutrino Oscillation

The concept of neutrino oscillation was first proposed by B. Pontecorvo in 1957, although his original proposal mainly describes the oscillation between neutrino and anti-neutrino. This is different from the concept of neutrino oscillation nowadays. To describe the phenomenon of neutrino oscillation, we should know that the neutrinos have two types of eigenstates, the flavor eigenstates and the mass eigenstates, and these two types of eigenstates are not necessarily identical. The flavor engenstates are the neutrino states created by lepton flavors (electron, muon, tau) via weak interactions. The detection of such states also result corresponding flavors of leptons by weak interactions. However, the mass eigenstates carry quantum numbers of energy and momentum obeying Einstein's relations. Between these two types of eigenstates, there exists an unitary transformation between them to guarantee the probability conservation. In the following, we shall give a discussion on neutrino oscillation.

1.2.1 Neutrino Oscillation in Vacuum[10]

First we define two types of eigenstates,

$$\text{flavor eigenstate: } \begin{pmatrix} \nu_e \\ \nu_\mu \\ \nu_\tau \end{pmatrix}, \qquad \text{mass eigenstate: } \begin{pmatrix} \nu_1 \\ \nu_2 \\ \nu_3 \end{pmatrix} \tag{1.2}$$

There exist a unitary connecting flavor eigenstates and mass eigenstates.

$$\begin{pmatrix} \nu_e \\ \nu_\mu \\ \nu_\tau \end{pmatrix} = U \begin{pmatrix} \nu_1 \\ \nu_2 \\ \nu_3 \end{pmatrix} = U_{23}U_{13}U_{12} \begin{pmatrix} \nu_1 \\ \nu_2 \\ \nu_3 \end{pmatrix} \tag{1.3}$$

where

$$U_{23} = \begin{pmatrix} 1 & 0 & 0 \\ 0 & \cos\theta_{23} & \sin\theta_{23} \\ 0 & -\sin\theta_{23} & \cos\theta_{23} \end{pmatrix}, \quad U_{13} = \begin{pmatrix} \cos\theta_{13} & 0 & \sin\theta_{13} \\ 0 & 1 & 0 \\ -\sin\theta_{13} & 0 & \cos\theta_{13} \end{pmatrix}, \tag{1.4}$$

$$U_{12} = \begin{pmatrix} \cos\theta_{12} & \sin\theta_{12} & 0 \\ -\sin\theta_{12} & \cos\theta_{12} & 0 \\ 0 & 0 & 1 \end{pmatrix} \tag{1.5}$$

The U is so-called "mixing matrix", and $\theta_{\rm ij}$ is the "mixing angle".[1]

While a neutrino propagate in space, it must obey the Schrödinger equation. Due to the smallness of neutrino mass, the velocity of neutrino must be very close to the light speed. The relation of E(energy), p(momentum) and m(mass) can be expressed as

$$E = \sqrt{p^2 + m^2} \tag{1.6}$$

For $p \gg m$, we obtain

$$E \simeq p + \frac{m^2}{2p} \tag{1.7}$$

Using the substutution $p \longrightarrow -i\frac{\partial}{\partial r}$, $E \rightarrow i\frac{\partial}{\partial t}$, and $p \simeq E$, we obtain

$$-i\frac{\partial}{\partial r}\begin{pmatrix} \nu_1 \\ \nu_2 \\ \nu_3 \end{pmatrix} = \left[E + \frac{1}{2E}\begin{pmatrix} {m_1}^2 & 0 & 0 \\ 0 & {m_2}^2 & 0 \\ 0 & 0 & {m_3}^2 \end{pmatrix}\right]\begin{pmatrix} \nu_1 \\ \nu_2 \\ \nu_3 \end{pmatrix} \tag{1.8}$$

Then, we subtract E and $\frac{m_1^2}{2E}$ from the Eq. 1.8[2], and get a new equation

$$-i\frac{\partial}{\partial r}\begin{pmatrix} \nu_1 \\ \nu_2 \\ \nu_3 \end{pmatrix} = \left[\frac{1}{2E}\begin{pmatrix} 0 & 0 & 0 \\ 0 & \Delta m^2_{21} & 0 \\ 0 & 0 & \Delta m^3_{31} \end{pmatrix}\right]\begin{pmatrix} \nu_1 \\ \nu_2 \\ \nu_3 \end{pmatrix} \tag{1.9}$$

[1]Here, we do not discuss the CP violation phase for simplicity

[2]This does not affect the probability, since it simply renders us a constant phase. While calculating the probability for a specific neutrino, the phase will be canceled out.

The plane-wave solution of Eq. 1.9 can be easily obtained

$$\begin{pmatrix} \nu_1 \\ \nu_2 \\ \nu_3 \end{pmatrix}_r = \begin{pmatrix} 1 & 0 & 0 \\ 0 & e^{-i\frac{\Delta m^2_{21}}{2E}r} & 0 \\ 0 & 0 & e^{-i\frac{\Delta m^2_{31}}{2E}r} \end{pmatrix} \begin{pmatrix} \nu_1 \\ \nu_2 \\ \nu_3 \end{pmatrix}_{r=0} \tag{1.10}$$

Since we concern the evolution flavor eigenstates. We rewrite Eq. 1.10

$$U^{-1} \begin{pmatrix} \nu_e \\ \nu_\mu \\ \nu_\tau \end{pmatrix} = \begin{pmatrix} 1 & 0 & 0 \\ 0 & e^{-i\frac{\Delta m^2_{21}}{2E}r} & 0 \\ 0 & 0 & e^{-i\frac{\Delta m^2_{31}}{2E}r} \end{pmatrix} U^{-1} \begin{pmatrix} \nu_e \\ \nu_\mu \\ \nu_\tau \end{pmatrix}_{r=0} \tag{1.11}$$

To calculate the survival probability of ν_e, it is convenient to define,

$$U_{23}{}^{-1} \begin{pmatrix} \nu_e \\ \nu_\mu \\ \nu_\tau \end{pmatrix} = \begin{pmatrix} \nu_e \\ \nu_+ \\ \nu_- \end{pmatrix}, \quad \begin{aligned} \nu_- &= \cos\theta_{23}\nu_\mu - \sin\theta_{23}\nu_\tau \\ \nu_+ &= \sin\theta_{23}\nu_\mu + \cos\theta_{23}\nu_\tau \end{aligned} \tag{1.12}$$

In the basis, Eq. 1.10 then becomes

$$\begin{pmatrix} \nu_e \\ \nu_+ \\ \nu_- \end{pmatrix}_r = \begin{pmatrix} M_{11} & M_{12} & M_{13} \\ M_{21} & M_{22} & M_{23} \\ M_{31} & M_{32} & M_{33} \end{pmatrix} \begin{pmatrix} \nu_e \\ \nu_+ \\ \nu_- \end{pmatrix}_{r=0} \tag{1.13}$$

which $M_{\rm ij}$ is the matrix element of the i-th row and j-th column. Their values are

$$\begin{aligned} M_{11} &= C_{13}{}^2 C_{12}{}^2 + C_{13}{}^2 S_{12}{}^2 e^{-i\frac{\Delta m^2_{21}}{2E}r} + S^2_{13} e^{-i\frac{\Delta m^2_{31}}{2E}r} \\ M_{12} &= -C_{13}C_{12}S_{12} + C_{13}C_{12}S_{12}e^{-i\frac{\Delta m^2_{21}}{2E}r} \\ M_{13} &= -C_{13}S_{13}C_{12}{}^2 - C_{13}S_{13}S_{12}{}^2 e^{-i\frac{\Delta m^2_{21}}{2E}r} + C_{13}S_{31}e^{-i\frac{\Delta m^2_{31}}{2E}r} \\ M_{21} &= -C_{13}C_{12}S_{12} + C_{13}C_{12}S_{12}e^{-i\frac{\Delta m^2_{21}}{2E}r} \\ M_{22} &= S_{12}{}^2 + C_{12}e^{-i\frac{\Delta m^2_{21}}{2E}r} \\ M_{23} &= S_{13}S_{12}C_{12} - S_{13}C_{12}S_{12}e^{-i\frac{\Delta m^2_{21}}{2E}r} \\ M_{31} &= -C_{13}S_{13}C_{12}{}^2 - C_{13}S_{13}S_{12}{}^2 e^{-i\frac{\Delta m^2_{21}}{2E}r} + C_{13}S_{31}e^{-i\frac{\Delta m^2_{31}}{2E}r} \\ M_{32} &= S_{13}C_{12}S_{12} - S_{13}S_{12}C_{12}e^{-i\frac{\Delta m^2_{21}}{2E}r} \\ M_{33} &= C_{13}{}^2 C_{12}{}^2 + C_{13}{}^2 S_{12}{}^2 e^{-i\frac{\Delta m^2_{21}}{2E}r} + S^2_{13} e^{-i\frac{\Delta m^2_{31}}{2E}r} \end{aligned} \tag{1.14}$$

where

$$\begin{aligned} C_{\rm ij} &= \cos\theta_{\rm ij} \\ S_{\rm ij} &= \sin\theta_{\rm ij} \\ \Delta m^2_{\rm jk} &\equiv m^2_{\rm j} - m^2_{\rm k} \end{aligned} \tag{1.15}$$

We now can calculate the survival probability, $P(\nu_e \to \nu_e)$. Because $P(\nu_e \to \nu_e)$ only involve M_{11}, only M_{11} will appear in the following calculation for simplicity.

$$\begin{aligned} P(\nu_e \to \nu_e) &= |\langle \nu_e(r) | \nu_e(r=0) \rangle|^2 \\ &= \left| \begin{pmatrix} 1 & 0 & 0 \end{pmatrix} \begin{pmatrix} {C_{13}}^2{C_{12}}^2 + {C_{13}}^2{S_{12}}^2 e^{-i\frac{\Delta m^2_{21}}{2E}r} + S^2_{13} e^{-i\frac{\Delta m^2_{31}}{2E}r} & \cdots & \cdots \\ \vdots & \ddots & \\ \vdots & & \ddots \end{pmatrix} \begin{pmatrix} 1 \\ 0 \\ 0 \end{pmatrix} \right|^2 \\ &= 1 - C^4_{13}\sin^2 2\theta_{12}\sin^2\Delta_{21} - C^2_{12}\sin^2 2\theta_{13}\sin^2\Delta_{31} - S^2_{12}\sin^2 2\theta_{13}\sin^2\Delta_{32} \end{aligned} \tag{1.16}$$

where

$$\Delta_{\rm jk} \equiv 1.267\Delta m^2_{\rm jk}({\rm eV}^2) \times 10^3 \frac{r({\rm km})}{E({\rm MeV})} \tag{1.17}$$

$$\tag{1.18}$$

r is the baseline in km, E the neutrino energy in MeV, and m_j the j-th antineutrino mass in eV. Eq. 1.17 is independent of the CP phase angle δ_{CP} and the mixing angle θ_{23}. The $P(\nu_e \to \nu_e)$ is the survival probability for ν_e. We can define the disappearance probability $P_{dis} = 1 - P(\nu_e \to \nu_e)$ to determine the baseline of the θ_{13} experiment.

The followings is the latest measurements of the mixing angles and mass-squared differences by Super-K[1, 2] and KamLAND[5, 6] respectively,

$$1.5 \cdot 10^{-3}\ {\rm eV}^2 < |\Delta m^2_{31}| < 3.4 \cdot 10^{-3}\ {\rm eV}^2,\ \sin^2 2\theta_{23} > 0.92. \tag{1.19}$$

with the best fit values given by $\sin^2 2\theta_{23} = 1$ and $\Delta m^2_{31} = 2.1 \cdot 10^{-3}$ eV^2 respectively.

$$7.21 \cdot 10^{-5}\ {\rm eV}^2 < \Delta m^2_{21} < 8.63 \cdot 10^{-5}\ {\rm eV}^2,\ 0.267 < \sin^2\theta_{12} < 0.371, \tag{1.20}$$

with the best fit values $\Delta m^2_{21} = 7.92 \cdot 10^{-5}$ eV^2 and $\sin^2\theta_{12} = 0.314$. The third mixing angle, θ_{13}, is small and has not yet been determined; the current experimental bound is $\sin^2 2\theta_{13} \lesssim 0.12 \sim 0.2$ at 90% confidence level from CHOOZ[17].

Chapter 2

The Daya Bay Experiment

To measure the neutrino mixing angle θ_{13}, we need enormous neutrino source. The reactors become candidates. A typical reactor with 3 GW of thermal power(3 GW_{th}) emits 6×10^{20} antineutrinos per second with energy up to 8 MeV. The Day Bay nuclear power complex is one of the most prolific sources of antineutrinos in the world. Currently with two pairs of reactor cores (Daya Bay and Ling Ao), separated by about 1.1 km, the complex generates 11.6 GW of thermal power; The thermal power will increase to 17.4 GW by early 2011 when a third pair of reactor cores (Ling Ao II) is put into operation and Daya Bay will be among the five most powerful reactor complexes in the world. The site is located adjacent to mountainous terrain, ideal for setting up underground detector laboratories that are well shielded from cosmic ray backgrounds. This site offers an exceptional opportunity for a reactor neutrino experiment optimized to perform a precision determination of $\sin^2 2\theta_{13}$ through a measurement of the relative rates and energy spectrum of reactor antineutrinos at different baselines.

The basic experimental layout of Daya Bay consists of three underground experimental halls, one far and two near, linked by horizontal tunnels. Figure 2.1 shows the detector module deployment at these sites.

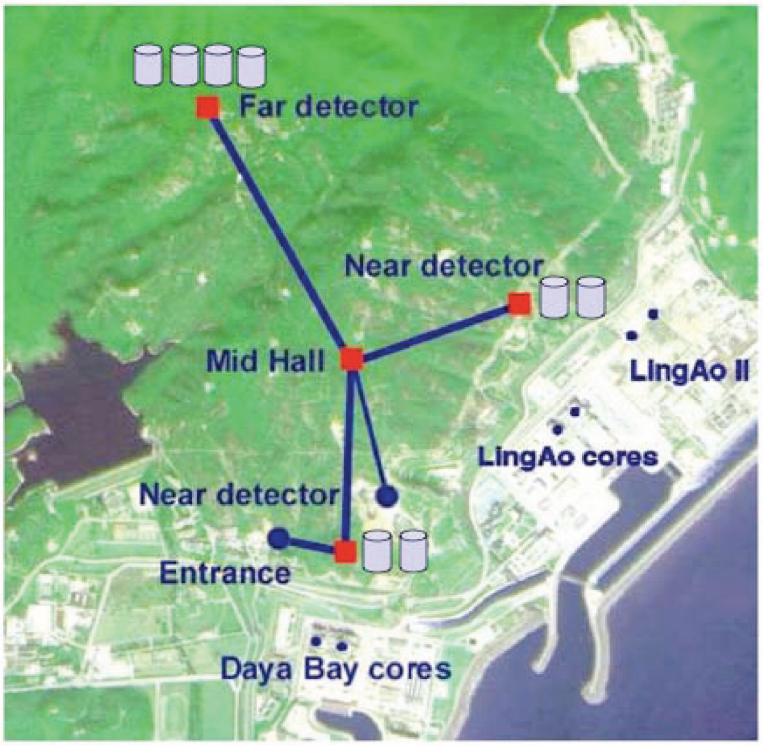

Figure 2.1: Default configuration of the Daya Bay experiment, optimized for best sensitivity in $\sin^2 2\theta_{13}$. Four detector modules are deployed at the far site and two each at each of the near sites.

2.1 The Optimization of Detector Baseline

We now use Eq. 1.17 to decide the baseline of the detector. In Eq. 1.17, we can divide the disappearance probability into two terms. The first term,

$$P_{12} = C_{13}^4 \sin^2 2\theta_{12} \sin^2 \Delta_{21} \approx \sin^2 \theta_{12} \sin^2 \Delta_{21} \tag{2.1}$$

for $\theta_{13} < 10^\circ$, which is only sensitive in θ_{12}. The second term,

$$P_{13} = C_{12}^2 \sin^2 2\theta_{13} \sin^2 \Delta_{31} + S_{12}^2 \sin^2 2\theta_{13} \sin^2 \Delta_{32} \tag{2.2}$$

is the term containing θ_{13}. To obtain the value of θ_{13} precisely, the Far detector should lay in the first oscillation maximum in θ_{13}. Fig 2.2 drawn with the best

fit parameters $\Delta m^2_{31} = 2.1 \cdot 10^{-3}$ eV^2, $\Delta m^2_{21} = 7.92 \cdot 10^{-5}$ eV^2, $\sin^2\theta_{12} = 0.314$, $\sin^2 2\theta_{13} = 0.10$ and E_ν=3.4 MeV, shows P_{13} dominate the survival probability of ν_e around $1 \sim 2$ km. As shown in Fig. 2.2, at the first oscillation maximum, which is about at $1 \sim 2$ km to the neutrino source, the P_{12} contribute least, i.e. $\sin^2\Delta_{21} \ll 1$. The P_{13} dominate the oscillation around this distance, and $P_{13} \approx \sin^2 2\theta_{13} \sin\Delta_{31}$, purely θ_{13} function.

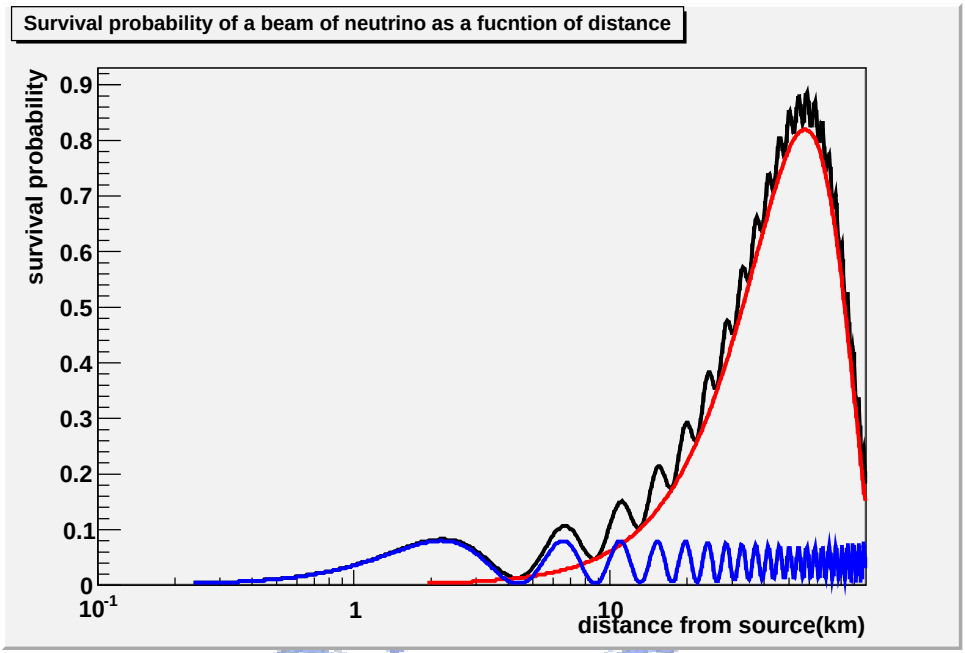

Figure 2.2: Reactor antineutrino survival probability as a function of distance from source. The black curve is the total disappearance probability, the red curve is the term P_{12} in disappearance probability, and the blue curve is the term P_{13} in disappearance probability.

2.2 Detection of $\bar{\nu}_e$ from Nuclear Reactor

The reaction employed to detect the $\bar{\nu}_e$ from a reactor is the inverse beta-deday $\bar{\nu}_e + p \rightarrow e^+ + n$. Neutrinos only have weak interaction and gravitational interaction. Even for the more sensitive interaction, weak interaction, the cross section is only 10^{-44}cm^2. In order to detect a free neutrino, the following requirements must be fulfilled[11]

1. a very intense neutrino source;
2. a proton-rich target;
3. a detection system designed to discriminate strongly aganist backgrounds because of the low event rate.

A nuclear reactor is a good candidate to provide strong neutrino source, because of average 6 neutrino emitted per fission. Using liquid scintillator, a proton-rich organic compound which can fluoresce upon the passage of an ionizing particle, as both a target and a detector, an antineutrino will give out measurable signals when the inverse beta decay occurs. Fig. 2.3 show how to detect inverse beta decay.

The sequence of physical processes in the diagram is as follows.

1. An antineutrino from the reactor interacts with a proton provided by the liquid scintillator and produces a positron with kinetic energy from zero to about 8 MeV, and a neutron with a negligible kinetic energy.
2. The positron is attracted by the surrounding negatively charged particles and is slowed down. Through diffusing in the liquid scintillator, the kinetic energy is transferred, producing scintillation light. Ultimately the positron annihilates with an orbital electron to give out two 0.511 MeV gamma. These processes take about 10^{-10} second and produce a prompt signal for the inverse beta decay.

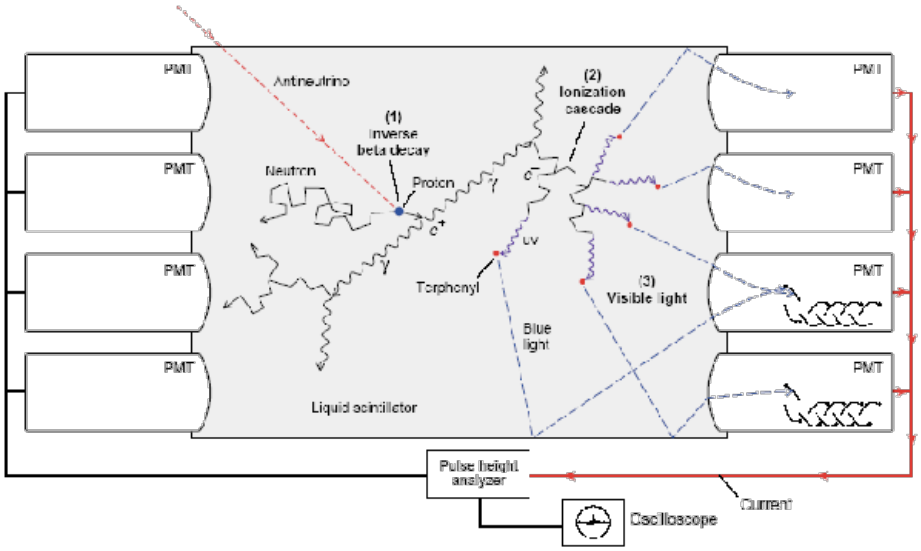

Figure 2.3: Schematic of antineutrino detector. An antineutrino interacts with a proton to give out a neutron and positron. Both particles produced then give out gamma rays.

3. The neutron is also slowed down by scattering with surrounding particles until it is captured by either hydrogen or doped chemicals. Then gamma rays will be emitted with characteristic energies and act as a delayed signal since these processes take about 10^{-5} second.

2.3 The Aberdeen Tunnel Experiment

To achieve the desired sensitivity to $\sin^2\theta_{13}$ of 0.01 or better, beside the highly sensitive equipment to detect neutrinos, it is necessary to discriminate the cosmic muon backgrounds from signal events. For Daya Bay experiment, it is highly desirable that these cosmic muon induced backgrounds be measured in an underground laboratory that has similar overburdens and rock types as those in the Daya Bay experiment.

The Aberdeen Tunnel laboratory in Hong Kong turns out to be a good location

for this purpose. It has an overhurden of approximately 250 m of rocks with similar composition to those in Daya Bay experiment. The laboratory is located at the cross junction of the tunnel tubes at the middle of the Aberdeen Tunnel in Hong Kong. It is 22 m above see level at 22.23°N and 114.6°E. Most of the rocks in Hong Kong Island is granite with an average density about 2.5 to 2.8 g/cm^{-3}.

The detector in Aberdeen Tunnel laboratory, it consists of a muon tracker and a neutron detector. The muon tracker is made up of three layers of proportional tubes and three hodoscopes of plastic scintillators for triggering on the cosmic-ray muons, and for determining the position of the incident muon in the offline analysis. The neutron detector contains two zones. The outer part is mineral oil to reduce the background such as γ-ray from radioactivity and cosmic moun-induced neutrons. The inner part is the liquid scintillator, which gives the signal when a neutron is captured. Fig. 2.4 shows the configuration of the Aberdeen Tunnel Lab.

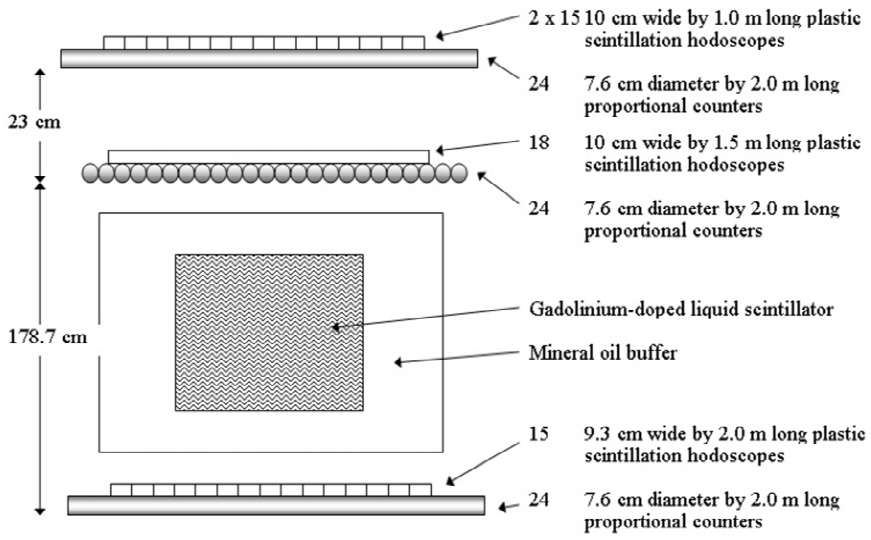

Figure 2.4: The detector configuration for studying the cosmic background at the Aberdeen Tunnel Laboratory.

Chapter 3

Estimation of the muon-induced neutrons

For the low energy neutrino experiments, fast neutrons from cosmic-ray muons known to be an important background. This is because the muon-induced neutrons often contaminate the neutrino detection signals . When an anti-neutrino is captured by inverse beta decay and a positron and a neutron are produced. The signals of anti-neutrino are detected by the detections of positions and neutrons. The muon-induced neutron often mimicked the signals, when it interacted with the detector. Unlike charged hadrons, which can be tagged by the veto system, neutrons can not be identified until they are finally captured.

In this chapter, we discuss the yield of muon-induced neutron, the neutron energy spectrum, and the neutron angular distribution by the Monte Carlo simulation package, FLUKA 2006.3, and we compare our result with that obtained by earler versions of FLUKA[12, 13, 16] and that by another simulation package, Geant4[1][14, 15, 16].

[1]This part of simulation has done by a colleague.

3.1 Background to Reactor Antineutrino Experiments

In reactor antineutrino experiments, the signal events (inverse beta decay reactions) have a distinct signature of two time-ordered events: a prompt signal resulting from position annihilation and a delayed neutron-captured signal. There are mainly two sources of neutron background in reactor antinetrino experiments. One is local radioactivity which forms the uncorrected background, and the other is cosmic-ray muon which forms the correlated one. The correlated background is defined in such a way that when a background event is triggered by the prompt signal and delayed signal, both signals come from the same source. For example, the the muon-induced neutron gives a delayed signal, and the recoiled proton gives prompt signal. On the contrary, the uncorrelated background is defined when two signals come from different sources but satisfy the trigger requirements by chance. For example, local radioactivity and the single neutron events induced by cosmic muons may occur within a time coincidence window accidentally to form an uncorrelated background. We can measure the neutron background from local radioactivity by changing the time coincidence window. The neutron yield from cosmic-ray muons strongly depends on the depth due to the energy loss of muon when penetrating into the underground site. The muon-induced neutron background is more important for such reactor antineutrino experiments. There are several reasons for this:

1. The muon-induced neutrons can mimic the neutrino event detected via the inverse beta decay interaction by a detector. When a fast neutron propagate in the detector, it interacts with the surrounding material and the proton in the nucleus recoils. the recoiled proton behave like a prompt signal of e^+. The fast neutron is then slowed down and finally captured that gives a delayed signal.

2. A detector can be protected against neutrons from the rock activity by

hydrogen-rich material, However such material will be a target for cosmic-ray muons and then produce more muon-induced neutrons surrounding the detector.

3. Cosmic-ray muons often have enough energy to penetrate through the detector and produce secondary particles, including secondary neutrons. But the primary particles will also interact with surrounding material and have the possibility to produce neutrons. These neutrons given by muon cascade make the background more complex and produce more fake signal events.

It is very difficult to measure these backgrounds, since they fulfill the whole requirements as an antineutrino event. In the ideal case, the background can be measured if the antineutrino sources, i.e. the nuclear reactors, are turned off. Obviously this is almost impossible. The simulation of muon-induced neutron is needed to give a rough estimation of the background. Before detailing the simulation, it is necessary to understand the origins of fast neutrons.

3.1.1 Origins of the fast neutrons

The primary cosmic ray particle interact with molecules of our atmospere producing hadronic showers. At sea level, about 75% of the particles are muons and others are pions, protons, neutrons, electrons, and gamma rays. Excpet muon, all of the above particles can not penetrate through rock top underground. This is why most of neutrino experiments are performed underground to protect their detectors against the contamination of cosmic ray.

As said, even other particles are blocked, there is still background coming from cosmic-ray muons. Fast neutrons from cosmic-ray muons are produced in the following processes.

1. Muon interactions with nuclei via a virtual photon producing a nuclear disintegrations, resulting in the original muon and a neutron coming out. This process is usually referred to as "muon spallation".

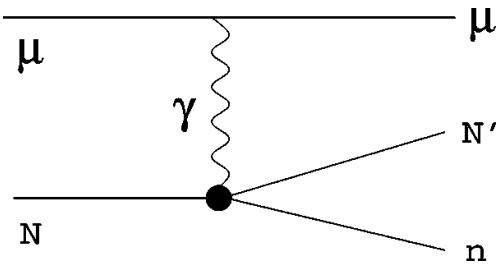

Figure 3.1: The Feynman diagram for a muon spallation process.

2. Muon elastic scattering with neutrons bound in nuclei.

3. Photonuclear reactions associated with eletromagnetic showers generated by muons.

4. There are secondary neutrons produced following any of the above processes.

3.2 Simulation of neutron production in hydrocarbon scintillator

In order to study neutron production by muon in materials we consider a μ^- beam with mono-energy and mono-direction incident at the center of a block filled with hydrocarbon scintillator. We choose $C_{10}H_{22}$ as the material for our this simulation. The density of $C_{10}H_{22}$ is 0.85 g/cm^3. The thickness of scintillator block depend on the energy of muon beams. For the muon beams with energy below 100 GeV, we choose the thickness as 1500 cm; for the muon with energy above 100 GeV, the thickness 4500 cm is chosen.

Muon-induced cascades require a certain length of material to develop and reach equilibrium in the number of neutrons produced per unit muon track length. To avoid the edge effect, neutron produced in the very beginning region are dropped off, only neutrons produced in the later region are considered.

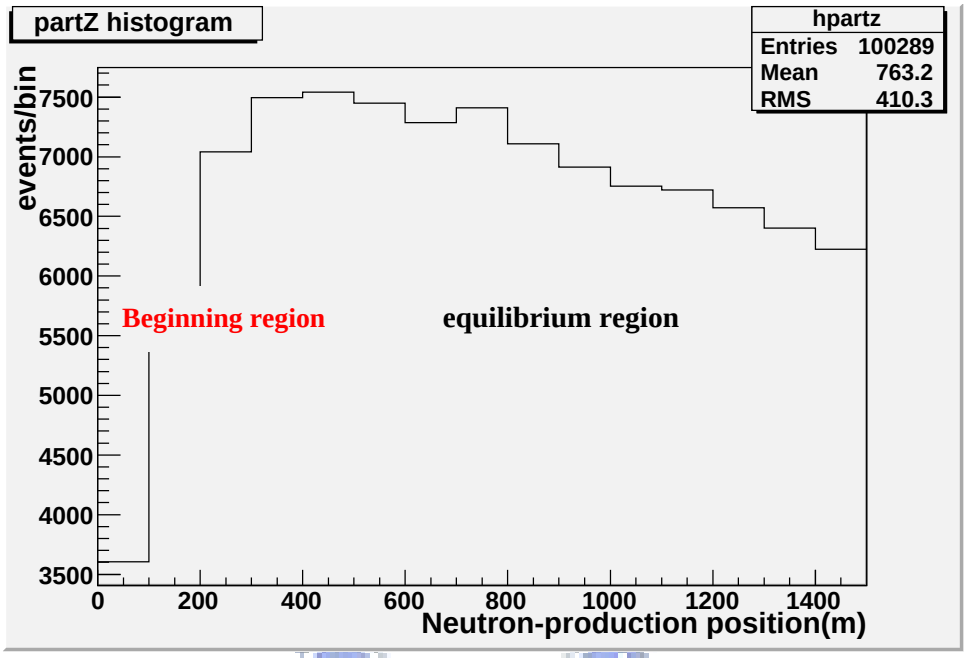

Figure 3.2: The histogram for neutron production positions by 10 GeV muons. It shows that the muon cascades reach equilibrium after the position 450 cm, the muon cascades reach equilibrium.

In Fig.3.2, the neutron production in the beginning is rapidly growing, because the muon cascade has not yet completely developed. Therefore the neutron production in this region are disregarded.

For muon energies below $\sim$ 100 GeV one must also correct for muon energy loss, as shown in Fig. 3.2. In the equilibrium region, the neutron production is slightly decreasing resulting from the muon energy loss. If we just take the initial muon energy to be representive the muon energy here. We shall miss the effect of the muon energy loss. To correct for the energy loss, it is reasonable to take the representative muon energy as the averaged muon energy in the equilibrium region.

In counting the number of neutrons created in a cascade, one must avoid double-counting. For the neutron-induced neutron interaction, FLUKA treats the parent neutron after interaction to be a new-born neutron. To avoid the double-countings, we consider that the highest energy one in the final state corresponds to the initial neutron and remove it from the count. The following figure illustrates this procedure.

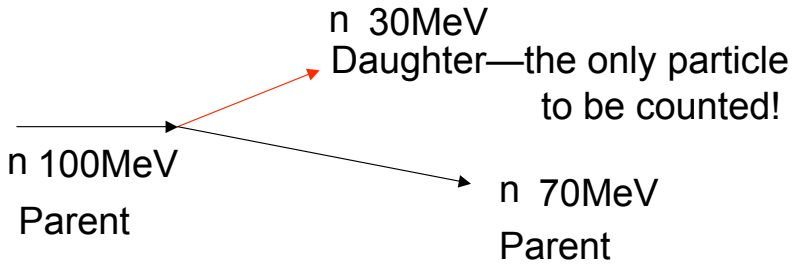

Figure 3.3: Illustration of neutron-induced neutron interaction

In Fig. 3.3, We show an example where a neutron with energy 100 MeV interacts with certain nucleus and produces two neutrons with energies 30 MeV and 70 MeV. We treat the neutron with energy 70 MeV to be the parent neutron, and the neutron with energy 30 MeV to be the daughter neutron. We only count the daughter neutron in this interaction.

3.3 Results

3.3.1 The neutron yield

The total neutron yield, as the function of muon energy, given by different sium-lations, are shown in Fig. 3.4. The parameterization of neutron yield in our simulation is

$$N_n = 4.82 \times \left(\frac{E_\mu}{\mathrm{GeV}}\right)^{0.69} \times 10^{-6}\mathrm{neutron}/\mu/(\mathrm{g/cm}^2) \tag{3.1}$$

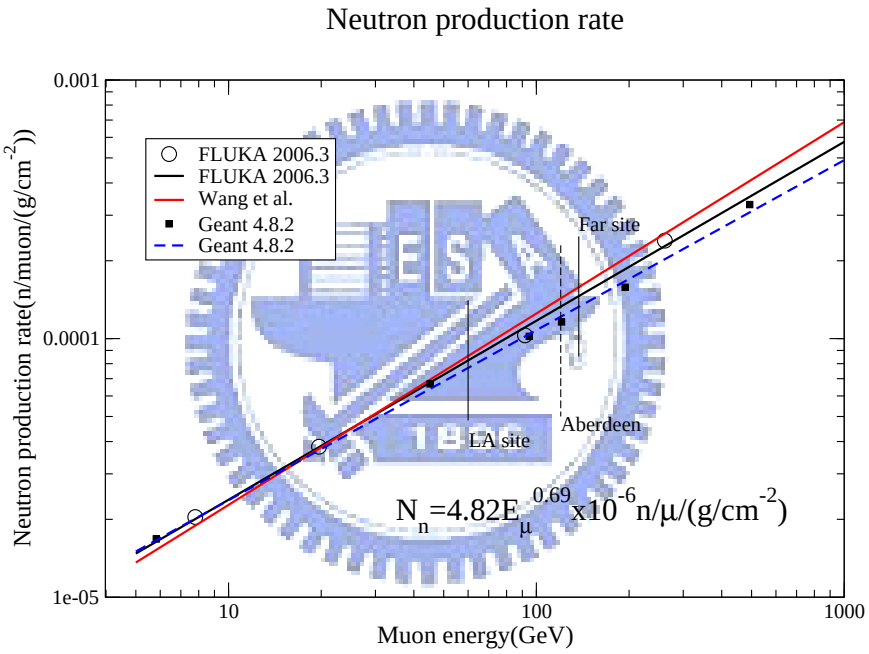

Figure 3.4: The neutorn yield as the function of muon energy. The horizontal axis is muon energy and the vertical axis is the events number per g-cm^{-2} per muon. The circle points are the data points of FLUKA 2006.3 and the black curve is the fitting. The red curve is the parameterization published by Wang et al.[13]. The square points are the data points of the Geant 4.8.2 and the blue dash line is the fitting.

In Fig. 3.4, in the low energy region(< 50GeV) three fitting curves are quite similar. However, in the region above 100 GeV, the result of FLUKA 2006.3 is smaller than that of Wang et al. by about 14%. The result of Geant4.8.2 is smaller than that of Wang et al. by about 30%.

Three vertical lines in Fig.3.4, indicate the average muon energy in every specific experimental sites, 130 GeV for the Far site, 60 GeV for the LingAo site, and 120 GeV for the Aberdeen site.

We use a simple formula to define the deviation between Geant4.8.2 and FLUKA 2006.3.

$$\text{Deviation} = \frac{\text{Geant4} - \text{FLUKA}}{\text{Geant4}} \times 100\%$$

	Aberdeen Tunnel	Ling Ao Near	Far Hall
Mean muon energy (GeV)	120	60	130
Deviation (%)	7.9	5	8

Table 3.1: The deviations on neutron yield predictions between two different simulation tool kits at the different experimental sites.

The deviations of both simulations in these experimental sites are rather small. It means that similar results from two different simulation packages can be obtained in this energy region. It is reasonable for the deviations ar small, because the muon energies of these sites is not large. In the previous figure, we have a conclusion that the difference become larger when the energy is around 1000 GeV. but these energies of this sites are only around 100 GeV.

By these simulations, one can estimate the neutron yields in these experimental sites. For example, we discuss the Aberdeen Tunnel experimental site. In the Aberdeen Tunnel, the muon average energy and the muon intensity are:

$$\langle E_\mu \rangle = 120.7 \text{ GeV}, \quad I_\mu = 9.66 \times 10^{-6} \text{cm}^{-2}\text{s}^{-1} \tag{3.2}$$

In the liquid scintillator $C_{10}H_{22}$, with the density 0.85g cm^{-3}, the neutron yield is

$$N_n^{LS} \simeq 1.0810 \times 10^{-3} \text{m}^{-3}\text{s}^{-1} \tag{3.3}$$

We expect about 93 neutrons per day per m^3 induced by the cosmic ray muons, and about 72 neutrons produced in the liquid scintillator of the Aberdeen Tunnel site. To get a more realistic estimation of neutron yield from cosmic muons, it is necessary to simulate the whole geometry of Aberdeen Tunnel experimental site. To do this, the full information on muon flux is needed, not the average one. The details will be discussed in the next chapter. The above is estimation gives us a rough number of neutron yield in liquid scintillator.

3.3.2 Neutron energy spectra

We also compare the neutron energy spectra with a universal empirical function obtained by Wang et al.. The following one is the empirical function is given by

$$\frac{dN}{dE_n} = A\left(\frac{e^{7E_n}}{E_n} + B\left(E_\mu\right)e^{-2E_n}\right), \tag{3.4}$$

where A is normalization factor and

$$B\left(E_\mu\right) = 0.52 - 0.58e^{-0.0099E_\mu} \tag{3.5}$$

Fig.3.5 shows that the neutron energy spectra fitted to the empirical function of Wang et al.. Except the lowest muon energy case, the results of FLUKA 2006.3 agrees well with the empirical function. Even in the lowest energy case, the result of FLUKA also agree with the original histogram of Wang et al.(see Fig. 3.6).

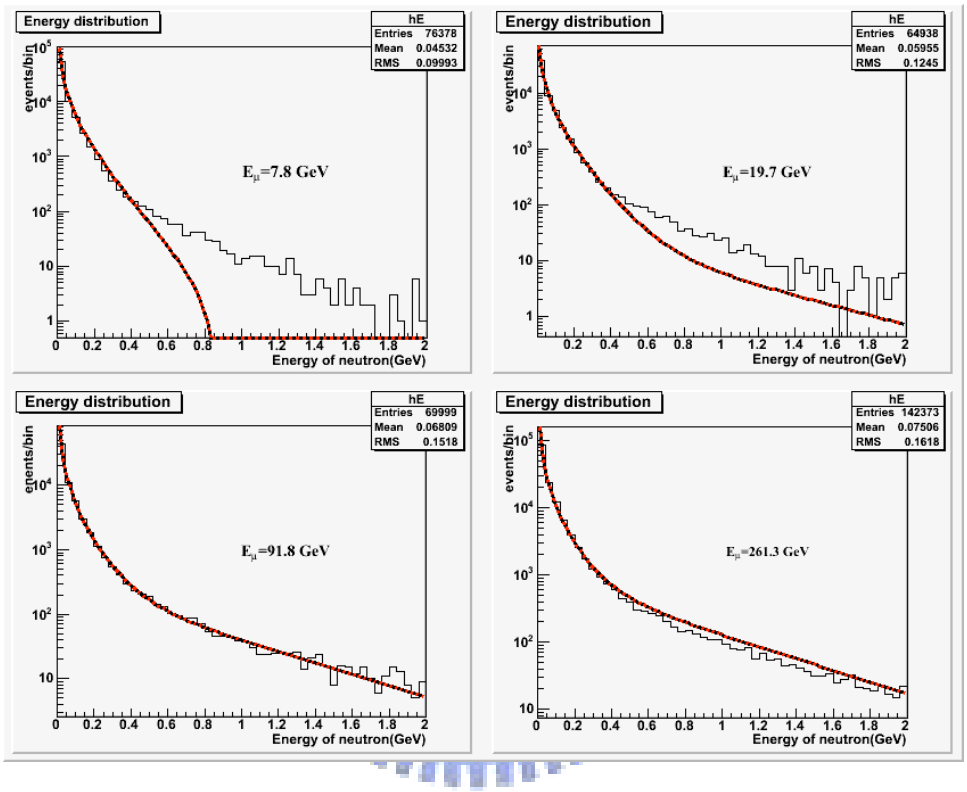

Figure 3.5: Neutron energy spectra at different primary muon energy: The black histograms are results of FLUKA 2006.3. The red curves are the empirical function of Wang et al..

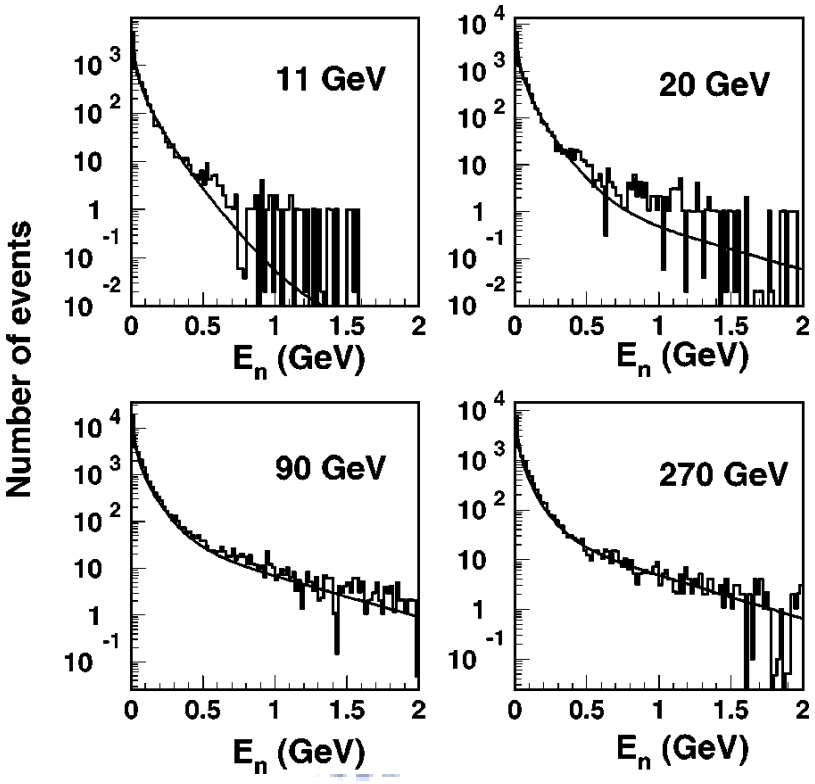

Figure 3.6: Neutron energy spectra at different primary muon energy obtained by Wang et al..

3.3.3 The neutron angular distribution

The neutron angular distribution relative to the primary muon track could help to understand the neutron background in any detector underground since muon tracks are relatively easy to reconstruct. It is expected to be forward peaked, smoothed somewhat by the contribution of secondary neutrons. We fitted our result with the parateterization obtained by Wang et al.

$$\frac{dN}{d\cos\theta} = \frac{C}{(1-\cos\theta)^{0.6} + D\left(E_\mu\right)} \tag{3.6}$$

where $D\left(E_\mu\right) = 0.699E_\mu^{-0.136}$. The results of FLUKA 2006.3 agree well with the parameterization of Wang et al..

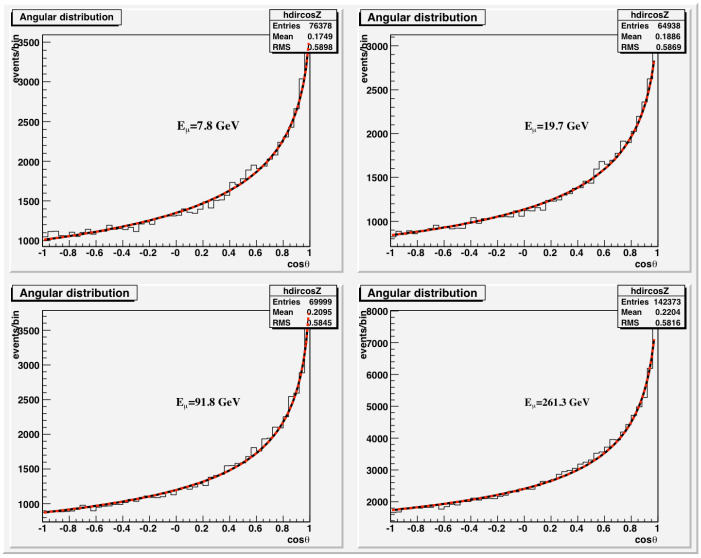

Figure 3.7: Neutron angular distribution. The horizontal axis is cosine of the angle between muon direction and neutron direction, and the vertical axis is the event number per bin. The histogram is the result of FLUKA 2006.3 and the red curves are the parameterization of Wang et al..

3.3.4 Origins of neutrons

We have also analysed the importance of individual neutron-producing processes in this simulation, which can be compared to similar data from Geant4, and prevous version of FLUKA. The following two figures present the relative contribution by each process as a function of the muon energy, which are obtained by FLUKA 2006.3 and Geant4 respectively.

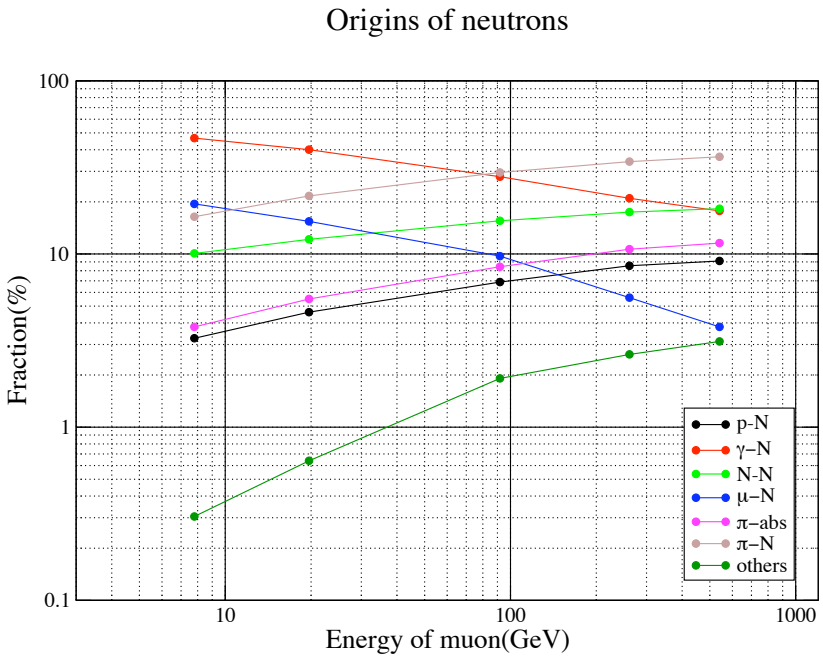

Figure 3.8: origins of neutrons sinulated by FLUKA 2006.3

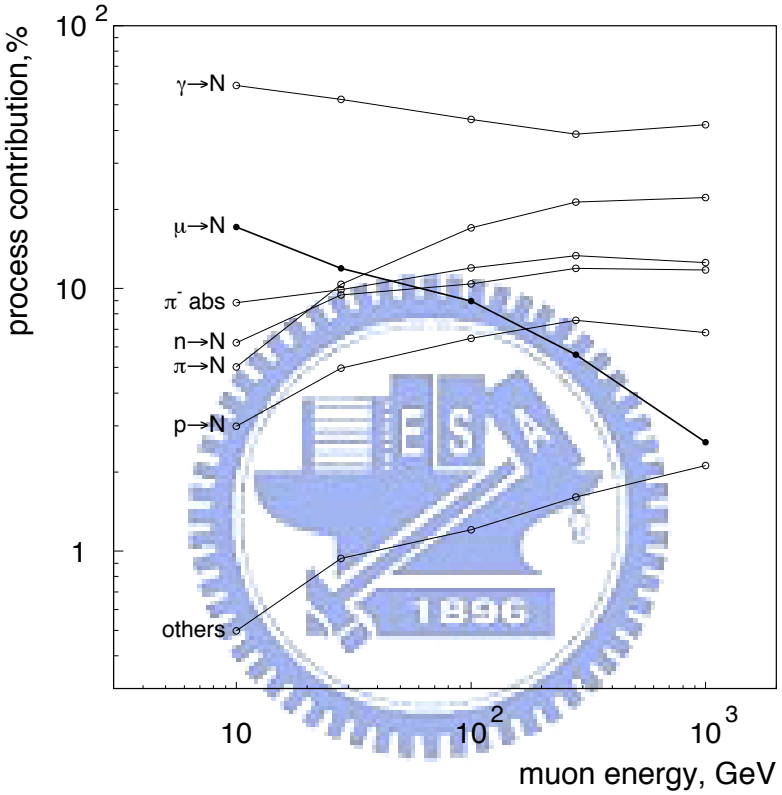

Figure 3.9: Origins of neutrons simulated by Geant4

There is a certain similarity agreement between two results, in that both predict neutron production by electromagnetic cascades (real photonuclear interaction) dominate at lower energies and decrease in its importance with an increasing muon energy, while neutron production by hadronic cascades become more important with an increasing muon energy. In those two figures, the most significant difference in between two simulation packages is on the $\pi - N$ process. In the low energy range, the fraction of $\pi - N$ given by FLUKA is 3 times larger than that given by Geant4. In the high energy range, the fraction of $\pi - N$ by FLUKA is 1.5 times larger than that by Geant4.

Chapter 4

The Prediction of Neutron Yield by Cosmic Muons in Aberdeen Tunnel Site

If we simply score the calculation of the previous chapter, there will be about 72 neutrons produced in the liquid scintillator of the Aberdeen Tunnel site. However, the estimation only treat the cosmic muons as mono-directional and mon-energetic. Furthermore, we only use a simple geometry in that the simulation, a cube filled will liquid scintillator, instead of the realistic geometry. In this chapter, we will discuss the realistic situation in the Aberdeen Tunnel site.

4.1 Cosmic-ray Muon Distribution in Aberdeen Tunnel Site

Before simulating the neutron yield in the Aberdeen Tunnel site. We need the muon flux and spectrum in the Aberdeen Tunnel site. We use the Modified Gaisser formula to get the sea-level muon spectrum and generate random events using the

Monte Carlo method. The Modified Gaisser formula is

$$\frac{dN_\mu}{dE_\mu} \simeq \frac{0.14 E_\mu^{-2.7}}{\text{cm}^2\text{s sr GeV}} \left(1 + \frac{3.64}{E_\mu g(\theta)}\right)^{-2.7} \left(\frac{1}{1 + \frac{1.1 E_\mu g(\theta)}{115}} + \frac{0.054}{1 + \frac{1.1 E_\mu g(\theta)}{850}}\right) \tag{4.1}$$

where,

$$g(\theta) = \sqrt{\cos^2\theta + {P_1}^2 + P_2 \cos^{P_3}\theta + P_4 \cos^{P_5}\theta} \tag{4.2}$$

and

$$P_1 = 0.102573, P_2 = -0.068287, P_3 = 0.958633, P_4 = 0.1817285, P_5 = 0.817285 \tag{4.3}$$

Then the MUSIC(MUon SImulation Code) is used to simulate the propagating of muons through rock in Aberdeen Muontain and the energy loss of each interaction via different physical processes. The propagation length is given by the distance from the mountain surface to the underground laboratory. Fig. 4.1 illustrates the Aberdeen Mountain with the underground laboratory located at $(0, 0, 22\text{m})$.

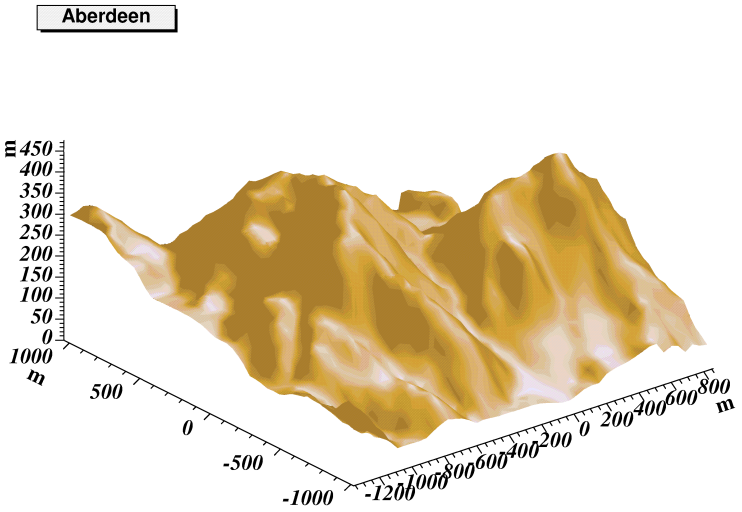

Figure 4.1: Aberdeen Mountain 3D scheme

Using the Modified Gaisser formula and MUSIC simulation package, we can get the muon flux and energy spectrum. Fig. 4.2 and Fig. 4.3 show the energy

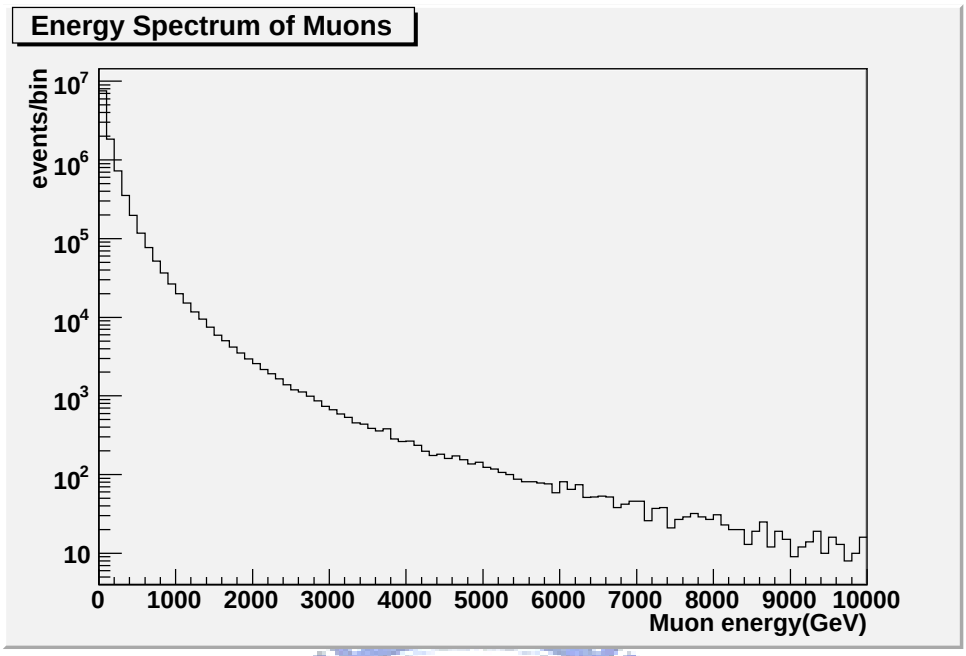

Figure 4.2: Muon energy sepctrum in Aberdeen Tunnel site

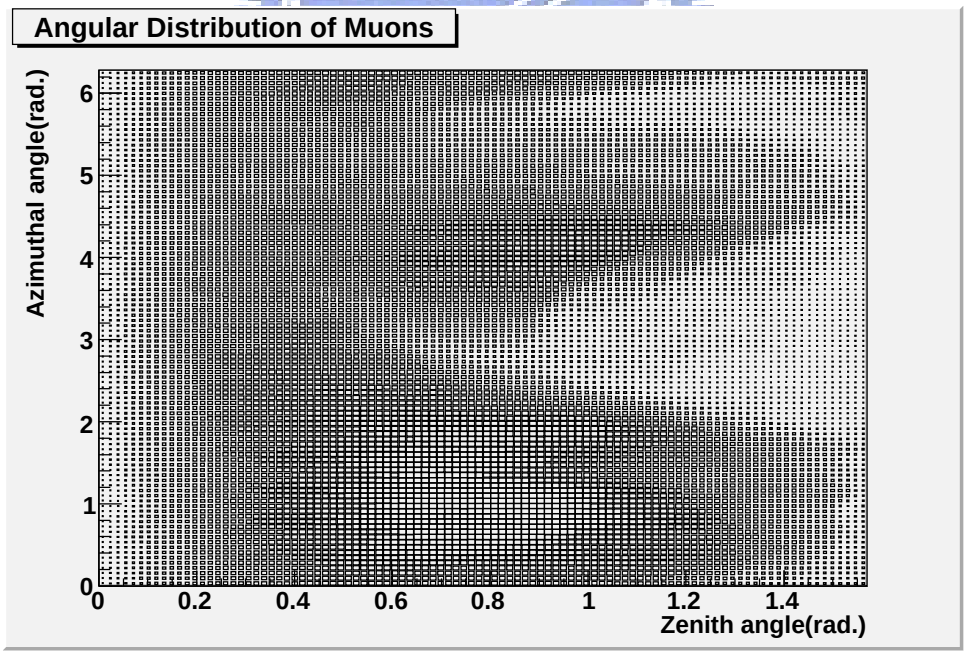

Figure 4.3: Muon angular distribution at the Aberdeen Tunnel site

spectrum and the angular distribution. The average energy of muon flux and the integrated muon intensity are

$$\langle E_\mu \rangle = 117.7 \text{ GeV}, \quad I_\mu = 1.085 \times 10^{-5} \text{cm}^{-2}\text{s}^{-1} \tag{4.4}$$

4.2 Neutron yield in Aberdeen Tunnel site

4.2.1 Configuration

Before discussing the configuration of the simulation, we set the center point to be the ground point of the center of the liquid scintillator. The +y direction point at north. To ensure muon cascade achieve the equilibrium, the muon first propagate through a block of rock with 10 m of thickness before reaching to the underground laboratory. Therefore, it will be shot at 12.3 m high, which is the sum of the rock thickness and height of the laboratory, and its x and y values will be given radomly in a $(10 \times 10 \text{ m}^2)$ area$(-5 \text{ m} < x, y < 5 \text{ m})$ to guarantee simulating all directions of muons. The direction and energy of muons is given by the Modified Gaisser formula and MUSIC package. All properties of muons are input in FLUKA 2006.3.

There are three layers of muon trackers, with the dimension 200 cm $\times$ 200 cm $\times$ 10.54 cm. While a muon goes through a muon tracker, FLUKA 2006.3 will record its properties. When the muon penetrates through all three layers of muon trackers, it will be recognized as a coincident muon. All of neutrons produced in the liquid scintillator as well as neutrons arriving at liquid scintillator from outsite will be recorded, and the neutron which go into the liquid scintillator from outside will be recorded, too.

While muons propagate in the Aberdeen Tunnel Laboratory, it is possible that some muons run out of the geometry set by the simulation, and consequently the program terminates. So the muon number which arrive the detector will be less than that generated in the initial position. But the muon flux around the detector should be approximately equal to that in the top of the geometry. To fix this

problem, the periodic boundary condition is employed. For example, while one particle escapes from the lab at +y wall, it shall return to the lab from the -y wall with the same physical properities.

4.2.2 Results

After simulating 2×10^6 muons in the Aberdeen Tunnel site, we obtain 17437 coincident muons and 208 neutrons produced in the liquid scintillator, in which 35 of these neutrons are produced by the coincident muons. By the previous discussion, we can easily calculate the time period for accumulating 2×10^6 muons. In fact, it would take 1.8433×10^5 seconds, roughly 2 days to accumulate these muons. Thus, there are an average number of 97 neutrons produced in liquid scintillator per day. Also, we find that there are 206 neutrons transporting into the liquid scintillator from ouside per day. Hence, there are totally 303 neutrons appearing in the liquid scintillator per day. The result by scaling numbers in the previous chapter, 72 neutrons/day does not include the neutrons transporting into the detector. Fig. 4.4 shows the energy distribution of the muon-induced neutrons, which include neutrons produced in liquid scintillator and tranporting into the liquid scintillator.

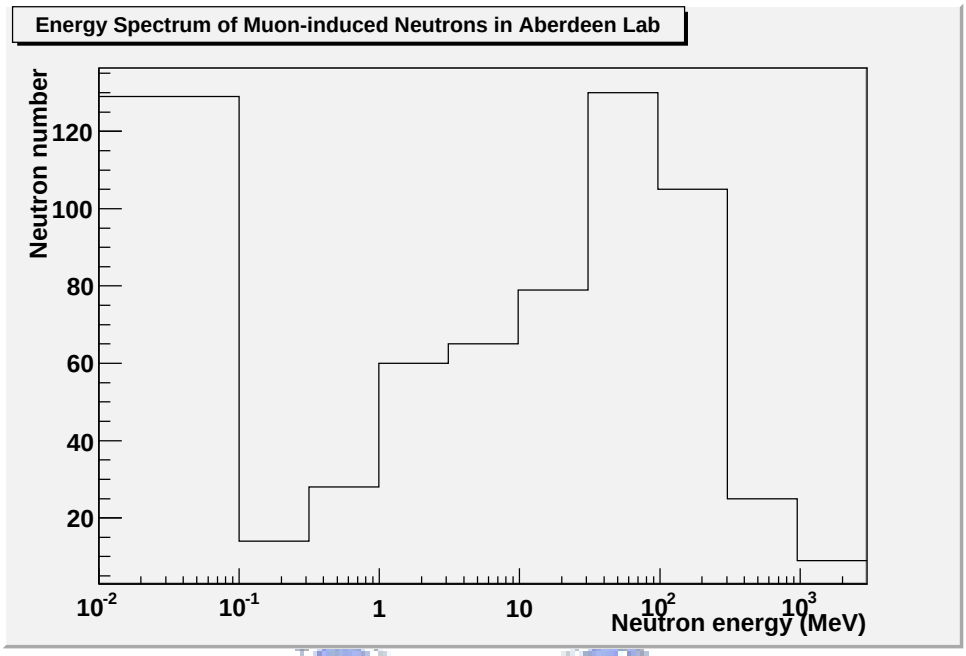

Figure 4.4: The energy distribution of muon-indued neutron which contain neutrons transporting into liquid scintillator and those produced in liquid scintillator. The mean energy is 81.9 MeV.

Chapter 5

Conclusion and Outlook

We have introduced the brief history of neutrino and the importance of the neutrino physics. The neutrino mixing that confirms the non-zero mass of neutrino make physicists extend the Standard Model. We have also discussed the detection of neutrinos and the backgrounds in neutrino experiments. Due to the deficult detection of neutrino, it is necessary to study backgrounds carefully to reduce errors coming from the backgrounds. This shows the importance of the Aberdeen Tunnel Experiment for the success of Daya Bay Neutrino Experiment. This thesis mainly focus on the simulation of comic muon-induced neutron background. We also compared the muon-induced neutron simulations between various simulation tool kits: FLUKA 1999, FLUKA 2006.3 and Geant 4.8.2, and obtained a parameterization formula using FLUKA 2006.3

$$N_n = 4.82 \times \left(\frac{E_\mu}{\mathrm{GeV}}\right)^{0.69} \times 10^{-6}\mathrm{neutron}/\mu/(\mathrm{g/cm^2}). \tag{5.1}$$

We have used the parameterization formula to estimation that there are 72 neutrons produced in liquid scintillator in Aberdeen Tunnel Lab. Furthermore, we have cosidered the realistic situation, using Modified Gaisser Formula to generate the muon flux in the atmosphere and inputting the MUSIC to get the muon flux in Aberdeen Tunnel Lab. Finally, we have found that there are 97 neutrons produced in the liquid scintillator, and 206 neutrons transporting into the detector per day.

Comparing the results of estimation of neutron yield by parametrization formula and relastic simulation, we found the results of the two methods are similar for neutrons produced in the liquid scintillator. However, Eq. can not estimate the number of neutrons transporting to the liquid scintillator.

In the future, we will simulate the photon signals arising from the neutron capture, and the neutron detection efficiency.

Bibliography

[1] Y. Ashie *et al.* [Super-Kamiokande Collaboration], Phys. Rev. D **71**, 112005 (2005) [arXiv:hep-ex/0501064].

[2] Y. Ashie *et al.* [Super-Kamiokande Collaboration], Phys. Rev. Lett. **93**, 101801 (2004) [arXiv:hep-ex/0404034].

[3] E. Aliu *et al.* [K2K Collaboration], Phys. Rev. Lett. **94**, 081802 (2005) [arXiv:hep-ex/0411038].

[4] M. H. Ahn *et al.* [K2K Collaboration], Phys. Rev. D **74**, 072003 (2006) [arXiv:hep-ex/0606032].

[5] K. Eguchi *et al.* [KamLAND Collaboration], Phys. Rev. Lett. **90**, 021802 (2003) [arXiv:hep-ex/0212021].

[6] T. Araki *et al.* [KamLAND Collaboration], Phys. Rev. Lett. **94**, 081801 (2005) [arXiv:hep-ex/0406035].

[7] X. Guo *et al.* [Daya Bay Collaboration], arXiv:hep-ex/0701029.

[8] http://theta13.phy.cuhk.edu.hk/

[9] T. Kajita [Super-Kamiokande Collaboration], Nucl. Phys. Proc. Suppl. **77**, 123 (1999) [arXiv:hep-ex/9810001].

[10] Yu-Chen Hsu, "The Oscillation Probabilities for Neutrino Traversing the Earth," Master Thesis, National Chiao Tung University (2005).

[11] Wah-kai Ngai, "Optimization and Background Studies for the Last Neutrino Mixing Angle θ_{13}," Master Thesis, The Chinese University of Hong Kong (2006).

[12] A. Ferrari, P. R. Sala, A. Fasso and J. Ranft,

[13] Y. F. Wang, V. Balic, G. Gratta, A. Fasso, S. Roesler and A. Ferrari, Phys. Rev. D **64**, 013012 (2001) [arXiv:hep-ex/0101049].

[14] V. N. Ivanchenko [Geant4 Collaboration], Nucl. Instrum. Meth. A **502**, 666 (2003).

[15] T. Mahmood, A. A. Zafar, T. Hussain and H. Rashid, AIP Conf. Proc. **888**, 301 (2007).

[16] H. M. Araujo, V. A. Kudryavtsev, N. J. C. Spooner and T. J. Sumner, Nucl. Instrum. Meth. A **545**, 398 (2005) [arXiv:hep-ex/0411026].

[17] M. Apollonio *et al.* [CHOOZ Collaboration], Phys. Lett. B **466**, 415 (1999) [arXiv:hep-ex/9907037].